Wave Run-Up and Air Gap Prediction for a Large-Volume Semi-Submersible Platform

Fabio T. Matsumoto
e-mail: fabio_matsumoto@tpn.usp.br

Rafael A. Watai
e-mail: rafael.watai@tpn.usp.br

Alexandre N. Simos
e-mail: alesimos@usp.br

TPN (Numerical Offshore Tank),
Department of Naval Architecture and Ocean Engineering,
Escola Politécnica,
University of São Paulo,
Av. Prof. Mello Moraes, 2231,
Cidade Universitária,
São Paulo, SP, 05508-900, Brazil

Marcos D. A. S. Ferreira
Research and Development Center (CENPES),
Petróleo Brasileiro S.A. (Petrobras),
Rio de Janeiro, RJ, Brazil
e-mail: marcos.donato@petrobras.com.br

This paper addresses the problem of estimating the air gap for a large semisubmersible production platform. Although it has a great impact on the design of the floating unit, many times the minimum deck height is still defined from simplified methods that incorporate relatively large safety margins. The reason for this is the intrinsic complexity of the associated hydrodynamic problem. Nonlinear effects on the incoming and scattered waves are usually relevant and sometimes nonlinear effects on the motions of the floating hull may also play an important role. This discussion is illustrated by means of wave basin tests performed with the model of a large semisubmersible designed to operate in Campos Basin. Significant run-up effects on its squared-section columns were observed for the steepest waves in several design conditions. Also, the unit presented relatively large low-frequency motions in heave, roll and pitch, which also affected the dynamic air gap measurements. In order to evaluate the difficulties involved in modeling such phenomena, simplified tests were also performed with the model fixed and moored in regular waves of varying steepness. Wave elevation in different points was measured in these tests and compared to the predictions obtained from two different numerical methods: a BEM code that incorporates second order diffraction effects (WAMIT) and a VOF CFD code (ComFLOW), the latter employed for fixed model tests only. Results show that a standard linear analysis may lead to significant errors concerning the air gap evaluation. Extending the BEM model to second order clearly improve the results as the wave-steepness increases. Although the VOF analysis is considerably time-consuming, simulations presented very good agreement to the experimental results, even for the steepest waves tested. [DOI: 10.1115/1.4007380]

1 Introduction

The deep water scenario of oil and gas exploitation in Brazil is one of the main factors that are driving engineers to develop a new generation of semisubmersibles (SS), characterized by having large displacement hulls. These platforms are stabilized by a four column arrangement and its position is maintained by polyester mooring-lines in taut leg configuration. In this context, in July 2008, Petrobras has started, with the Scientific Computing Research Network, a research project intended to improve knowledge and modeling of advanced hydrodynamics topics, such as the wave run-up phenomenon.

Brazilian experience is mostly based on two types of production systems: FPSOs and SS platforms. Concerning SS design, one of the main issues is defining its minimum air gap level, or, in other words, defining the minimum height of the lower deck in relation to the design waterline. Given the considerable impact that this level may have on the system budget, high accuracy prediction methods are very welcome, although they are not adequately established. The lack of numerical models and/or consistent methodologies with extensive experimental validation may result in unexpected problems during the validation stage or lead to the use of conservative safety factors.

There are various reasons that make the implementation of these methods even harder and they are related to the inherent complexity of the hydrodynamic problem. Once the design criteria for air gap definition are associated to extreme events, problems such as the nonlinearity of incoming and scattered waves play an important role. On SS platforms, one of the critical lower-deck areas are those surrounding the columns, frequently subjected to the wave run-up phenomenon. The intensity of this phenomenon is also directly linked to the wave steepness.

The influence of nonlinear effects brings serious implications in terms of numerical modeling of the phenomenon, which nowadays rests on numerical methods. There are several previous studies dealing with comparison of results obtained via the boundary element method (BEM), through the use of linear solution or including the effects of the second order diffraction. Stansberg et al. [1] presented wave run-up numerical predictions on different column-based platforms, identifying significant higher-order effects in the wave elevation from systematic variations in the wave steepness. A more recent work is the one presented by Danmeier et al. [2], which deals with the study of wave run-up on a gravity based platform by comparing results obtained via the WAMIT® code, [3] CFD, and experimental measurements, indicating significant differences in numerical results for large steepness waves.

Small-scale model tests of a large semisubmersible were carried out in the IPT (State of São Paulo Research Institute) towing tank in 2005. Tests were performed with fixed and moored models under the action of regular waves with different steepness, in order to verify the influence of this parameter on the free surface elevation below the model deck. Elevation was monitored by seven vertical wave probes. Simos et al. [4] presented a comparison between moored test results and those obtained from a standard first order numerical analysis. One of the main conclusions was that, although the linear approach presented a relatively good agreement for the design sea conditions tested, free surface elevation around the platform columns due to wave run-up was seriously underestimated.

Aiming at a better evaluation of the wave run-up problem, the present paper deals with the same experimental data, but extends the numerical analysis using the WAMIT second order module. In addition, CFD simulations using a volume of fluid (VOF) code

Contributed by the Ocean Offshore and Arctic Engineering Division of ASME for publication in the JOURNAL OF OFFSHORE MECHANICS AND ARCTIC ENGINEERING. Manuscript received July 26, 2010; final manuscript received May 11, 2012; published online February 22, 2013. Assoc. Editor: M. H. (Moo-Hyun) Kim.

Paper presented at the 29th International Conference on Ocean, Offshore and Arctic Engineering, Shanghai, China, 2010.

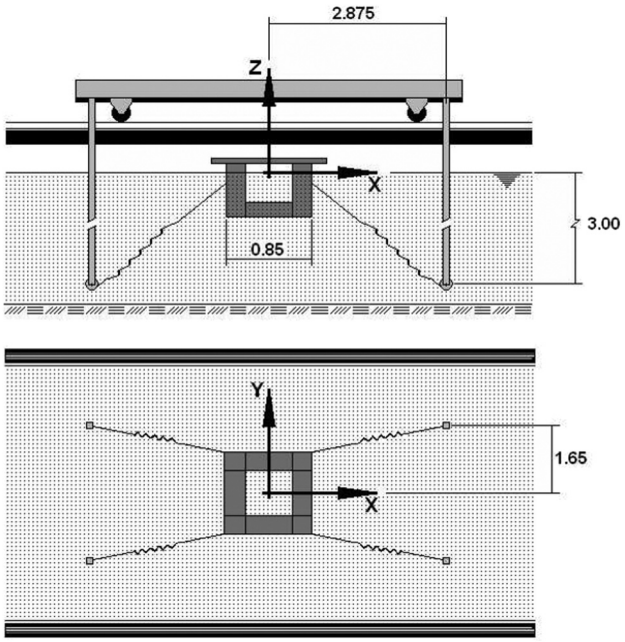

Fig. 1 Schematic representation of the experimental setup (dimensions in meters)

ComFLOW [5] were performed for the steepest waves in the fixed model test.

Experimental setup is briefly presented next, followed by a discussion on the numerical models.

2 Experimental Setup

Fixed and moored tests were conducted at the IPT towing-tank, which is 240 m long, 6 m wide, and 5 m deep. In a fixed test, the model was rigidly attached to the towing car. For the tests with the moored model, a supporting structure was built in order to accommodate submerged anchor points. To allow current emulation, this supporting structure was fixed to the carriage. The structure was designed for minimum disturbance of the incoming wave field and this was confirmed by a set of preliminary tests. Figure 1 presents a schematic view of the setup.

Since the new SS platforms are supposed to be moored in taut-leg configuration using polyester ropes, the restoring forces present a highly nonlinear behavior as a function of the platform horizontal excursions. Stiffness in pitch, roll, and yaw may vary significantly with the platform offset, as well as the surge-pitch and sway-roll coupling stiffness. Such variations may have an important influence on the air gap level and different experimental mooring arrangements were tested.

Preliminary tests were conducted with a simplified mooring arrangement provided by four linear springs, as illustrated in Fig. 1. The stiffness of each spring and the angles at the fairlead point were defined in order to reproduce characteristic values of surge and pitch stiffness of the full scale unit. Previous tests conducted using horizontal mooring lines and different wave directions indicated that the worst situations in terms of air gap demand occurred for bow waves.

The model scale was 1:100. The model main particulars presented in Tables 1 and 2 present the main parameters of the mooring system.

Analysis of decay tests and adjustments of first order motions provided the following mean values, presented in Table 3, of natural periods and linearized damping coefficients for the heave and pitch motion. Figures 2 and 3 present time traces of pitch and heave decay tests, respectively. The linearized damping coefficients were adjusted by the peak of the first order motion

Table 1 Model main characteristics

Characteristics	Model scale	Real scale	Unit
Length	0.850	85.0	m
Beam	0.850	85.0	m
Draught	0.275	27.5	m
Displacement	77.91	7.79×10^{7}	kg
Column width	0.175	17.5	m
Column breadth	0.175	17.5	m
Pontoon height	0.120	12.0	m
Pontoon breadth	1.750	175.0	m
Longitudinal center of gravity	0.000	0.0	m
Vertical center of gravity	0.250	25.0	m
Metacentric height	0.050	5.0	m
Transverse radius of gyr.	0.352	35.2	m
Longitudinal radius of gyr.	0.370	37.0	m

Table 2 Mooring system main parameters (model scale)

Characteristics	Value	Unit
Fairlead positions (X,Y,Z)	(±0.341, ±0.445, −0.060)	m
Anchor position (X,Y,Z)	(±2.875, ±1.646, −3.413)	m
Line stiffness	25.090	N/m

Table 3 Natural periods and damping

Motion	Tn (s) (Model scale)	Tn (s) (Full scale)	ζ (%)
Heave	2.29	22.9	6.0
Pitch	3.19	31.9	3.0

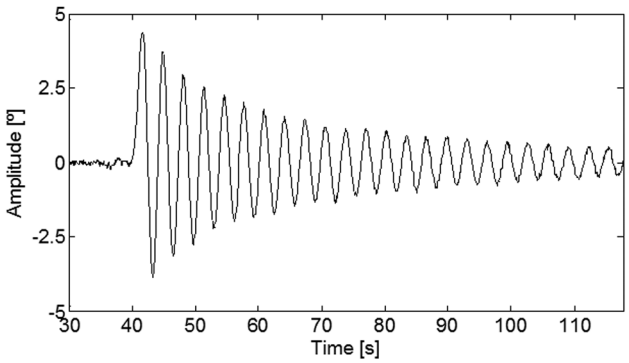

Fig. 2 Pitch decay test

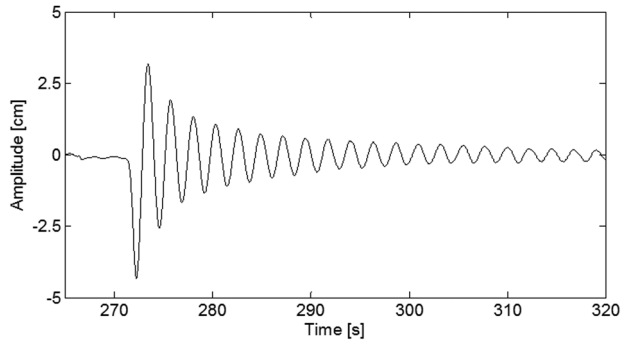

Fig. 3 Heave decay test

Table 4 Waves tested parameters (full scale)

Moored tests			Fixed tests		
Wave steepness (H/λ)	Wave amplitude (m)	Wave period (s)	Wave steepness (H/λ)	Wave amplitude (m)	Wave period (s)
1.59%	5.71	21.48	1.70%	6.12	21.48
2.07%	6.17	19.53	1.85%	5.62	19.73
2.78%	6.70	17.58	2.53%	6.11	17.58
4.02%	7.28	15.23	3.40%	6.16	15.23
3.98%	5.98	13.87	3.74%	5.61	13.87
5.54%	6.76	12.50	4.86%	5.56	12.11
4.90%	5.61	12.11	5.07%	5.80	12.11
6.13%	4.94	10.16	5.63%	6.23	11.91
6.17%	4.78	9.96	–	–	–

response operator obtained in the regular tests with the moored model.

Table 4 presents the wave parameters adopted in the tests for both moored and fixed tests (full scale). The tested wave periods comprehended a range between 21.48 and 9.96 s. As shown in Table 4, the variation on the wave steepness is mainly due to wave periods although the wave heights are not constant in the tests.

Motions in the six DOF were monitored along the tests. Surface elevation (relative to the hull) was measured by means of seven wave-probes (WP) fixed on the model. WP locations are depicted in Fig. 4.

With respect to Fig. 4, it should be noted that WP2, WP3, and WP4 were positioned in order to provide qualitative aspects concerning the wave run-up on the stern columns, which, as will be seen later, is a major concern with respect to this geometry.

3 Numerical Setup

In order to verify the nonlinear influence of wave steepness on the wave run-up and air gap, two numerical codes were selected. The first one is WAMIT which incorporates the second order effects on the scattered waves. The second one is ComFLOW, a VOF program for the numerical simulation of fluid flow, based on the Navier–Stokes equations. The software has been developed initially by the University of Groningen, The Netherlands, to study the sloshing of liquid fuel in spacecraft that in a microgravity environment requires a very accurate and robust improvement in the description of the free surface. This program introduces a local height function over the original VOF method, presented by Hirt and Nichols [6], bringing improvements to the free surface displacement calculations accuracy.

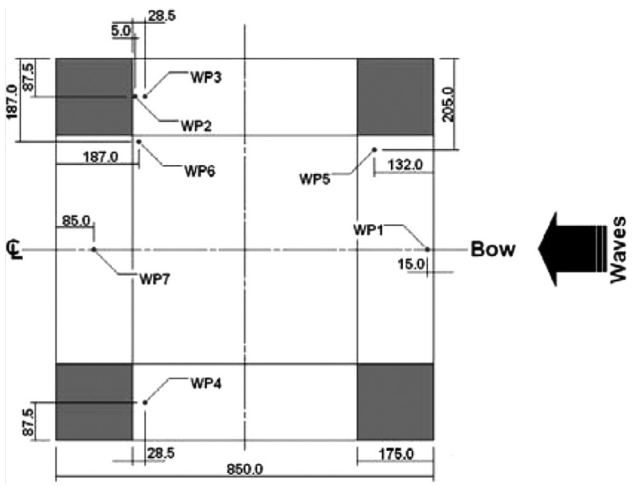

Fig. 4 Location of the wave-probes (values in mm)

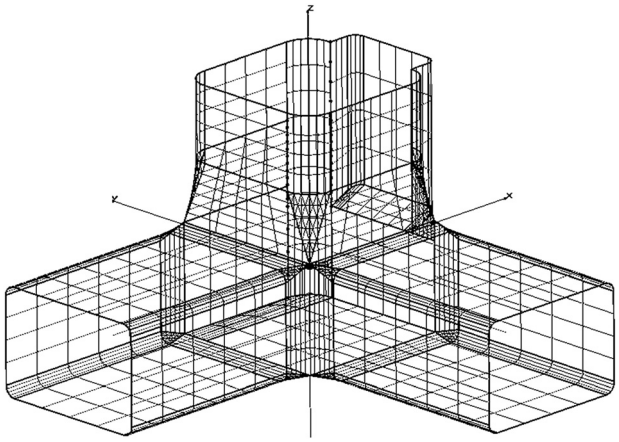

Fig. 5 WAMIT symmetrical model mesh (low order)

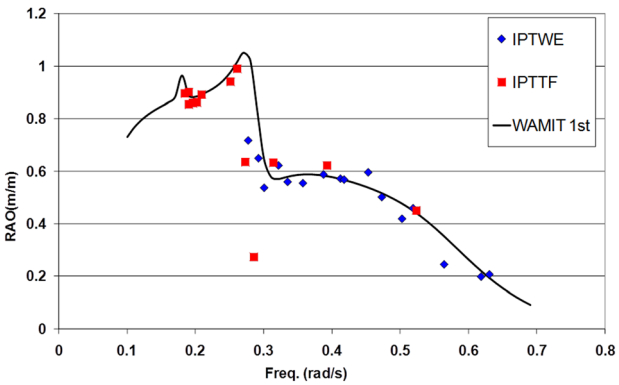

Fig. 6 Heave RAO (experimental and predicted results)

The WAMIT model is composed by the body surface and a free surface surrounding the body. The WAMIT body mesh was built using a 1356 panel mesh in accordance with the low order solver requirements. Although the platform has a slight asymmetrical component, in the WAMIT numerical model the symmetry was used in order to reduce processing effort. Figure 5 presents the symmetrical mesh used to perform the WAMIT computations. The convergence of the body mesh was verified through the first order motions adjustment presented in Figs. 6 and 7 for heave and pitch motion, respectively. As the numerical solution involves the calculation of second order effects, the free surface also needs to be discretized and convergence guaranteed. Basically, the second order total solution is composed by two terms; see for instance Pinkster [7]. The first one depends on the first order squared potential which the convergence can be associated directly with

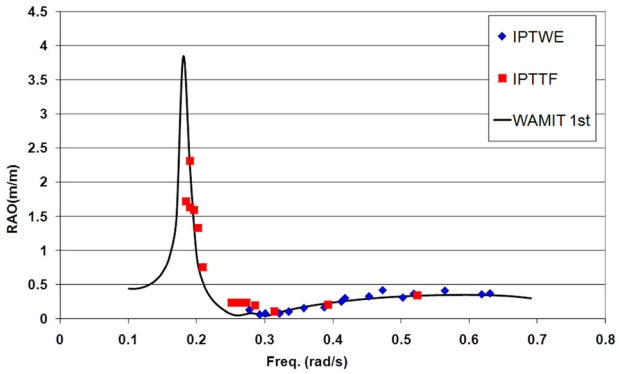

Fig. 7 Pitch RAO (experimental and predicted results)

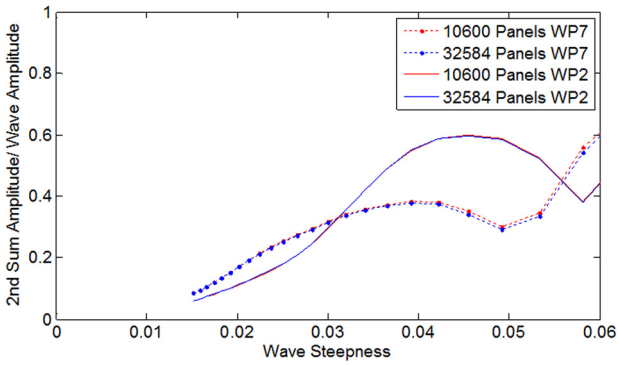

Fig. 8 Convergence analysis for second sum frequencies varying free surface panels

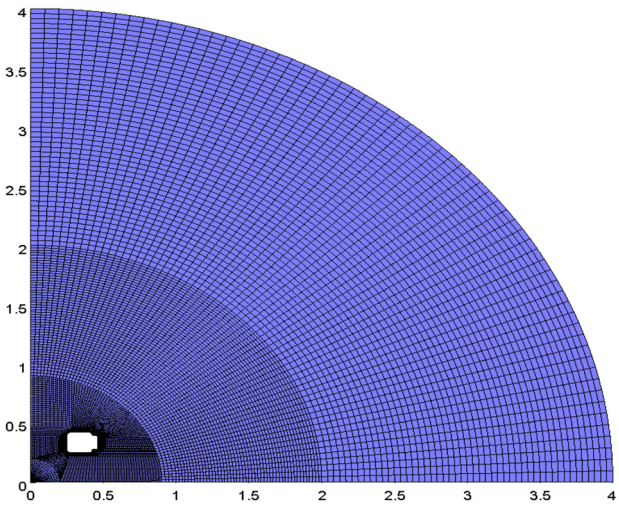

Fig. 9 Inner free surface mesh (10,600 panels)

the convergence of the first order potential. The second one is the second order potential which is associated with the source distribution over the free surface and its convergence must be verified through the variation of the free surface panel density near to the body. For defining the numerical mesh representing the free surface, an extensive convergence analysis was performed. According to Fig. 8, no representative difference was appointed when the number of panels varied from 10,600 to 32,584, indicating that the 10,600 panels mesh, illustrated in Figs. 9 and 10, is sufficient to represent the free surface forcing contribution. The so-called

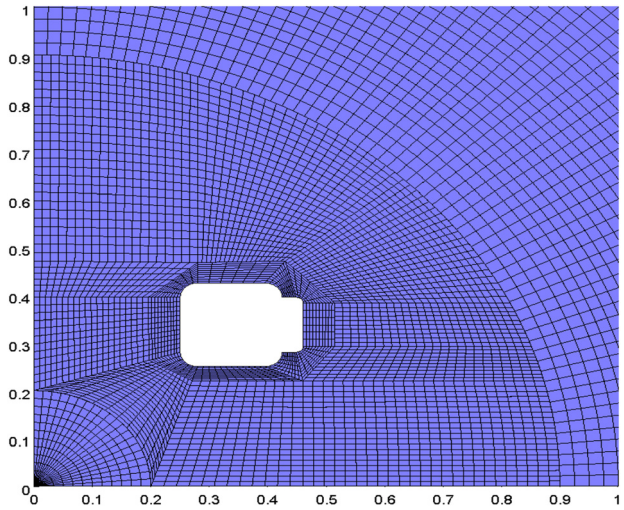

Fig. 10 Inner free surface details near to the column

inner radius was set to 4 ms and the asymptotic solution was truncated at 11 ms using 14 internal subdivisions.

For computing wave elevation respective to the moored-model tests, it is essential to obtain a good evaluation of the first order motions transfer functions. The experimental values of the RAOs for bow incidence were previously obtained through two different sets of regular wave tests. The first one (here named IPTWE) refers to the data obtained directly from the regular wave moored tests conducted for mapping the wave elevation (see Table 4). The second, here named IPTTF, was obtained in tests with longer waves, specifically carried out to determine the RAOs close to the resonant heave and pitch periods.

Figures 6 and 7 present the comparison between the experimental and theoretical values of the heave and pitch RAOs, respectively (frequency values converted to full-scale).

In the moored case, not only first order motions but also second order motions in low frequency can influence the air gap estimation. For a random sea incidence, the results of the tests showed that the second order motion is an important issue to predict the platform dynamic, see for instance, Simos et al. [8]. In order to provide a more consistent comparison between experimental and numerical results of air gap, the low frequency component in the regular wave tests (mean values) were also taken into account.

Obviously, high frequency effects may be disregarded concerning the motions of the platform. On the other hand, this effect should significantly impact the scattered wave elevation and consequently affect the air gap estimation. Therefore the numerical evaluation of free surface elevation includes the first order and both high and low frequency second order effects.

The first order free surface elevation is given by

$$\eta^{(1)} = -\frac{1}{g}\frac{\partial \phi^{(1)}}{\partial t} \tag{1}$$

where $\phi^{(1)}$ is the first order velocity potential that oscillates in the same frequency as the incoming wave. The second order free surface elevation evaluated by the WAMIT second order module is given by

$$\eta^{(2)} = -\frac{1}{g}\left(\frac{\partial \phi^{(2)}}{\partial t} + \frac{1}{2}\nabla\phi^{(1)} \cdot \phi^{(1)} - \frac{1}{g}\frac{\partial \phi^{(1)}}{\partial t}\frac{\partial^2 \phi^{(1)}}{\partial z \partial t}\right) \tag{2}$$

where $\phi^{(2)}$ represents the total second order velocity potential including diffraction and radiation effects when the platform is moored. The second order free surface elevation does not oscillate in the same frequency of the incoming waves but with double and

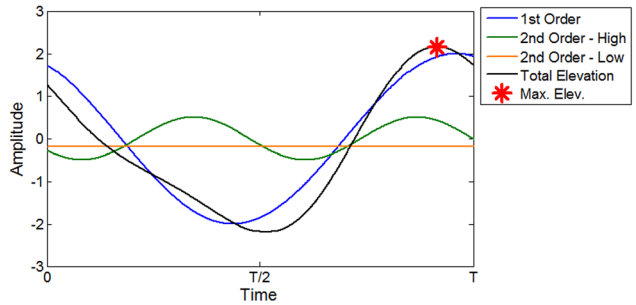

Fig. 11 Composition of the total free surface elevation

zero frequency, respectively, for the high and low frequency. Therefore, in order to obtain the maximum free surface elevation, each component was simulated and combined in the time-domain. Figure 11 illustrates the total free surface elevation composition.

Note that depending on the low frequency component phase in relation to the incoming wave its contribution diminishes the total free surface elevation. The low frequency component, as well as the high frequency component, can also increase or reduce the maximum free surface elevation. Thus, the maximum value obtained from the simulated signal is compared with the maximum value take from the experimental time series for each regular wave test.

The simulation results obtained with the modeling of the semisubmersible unit in the ComFLOW software followed several features which were indicated in the work presented by Iwanowski et al. [9].

ComFLOW has been already used for several applications within maritime areas, such as green water (see Kleefsmann et al. [10]), sloshing (see Bunnik and Veldman [11]) and wave run-up. Focusing in the latter, a vast number of works investigating the phenomenon in different platform units have been presented, see for instance, Buchner et al. [12], Loots and Buchner [13], Wellens et al. [14], and Iwanowski et al. [9].

The simulations were performed using regular waves with four different lengths to represent the incoming wave steepness described in Table 5. Each simulation comprised three wave periods. Some waves analyzed in the experimental tests were neglected because their characteristics were such that for a CFD analysis a large computational effort would be necessary to predict the results. Therefore, only the steepest waves were selected.

The fluid domain dimensions were chosen in order to keep the number of cells within reasonable figures. The computational domain length was defined to be $L = \lambda$, where λ is the incoming regular wavelength. The domain width was set to $B = 160$ m and symmetrical in relation to the centerline plane of the hull. Computational domain grid has been covered by cells of uniform size. The grid spacing in the horizontal plane was set to $\Delta X, Y \cong 0.5$ m and in the vertical directions the values were set to $\Delta Z \cong 0.8$. The number of cells in the computational domain were around $11–14 \times 10^6$ cells, leading to a very time-consuming analysis (approximately 15 days), as the algorithm does not yet allow parallel processing. Simulations were done in a computer equipped with a 2 QuadCore – Intel Xeon X5365 @ 3.00 GHz.

Table 5 ComFLOW waves simulated and total number of cells (full scale)

λ (m)	Height (m)	Period (s)	Steepness	ComFLOW total number of cells
300.36	11.22	13.87	3.74%	14892000
228.97	11.12	12.11	4.86%	11169000
228.97	11.60	12.11	5.07%	11169000
221.47	12.09	11.91	5.46%	10796700

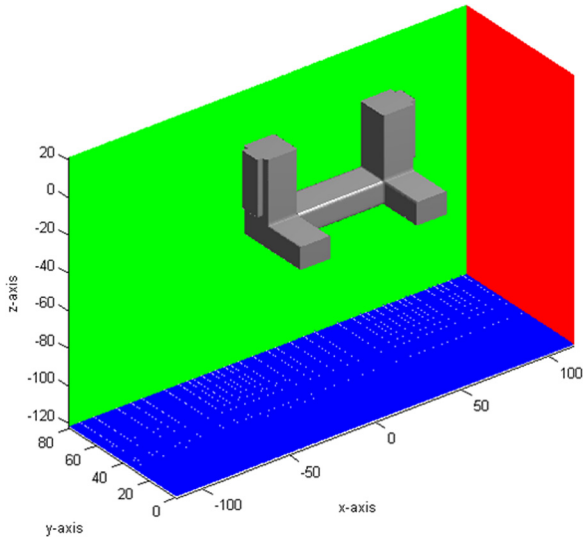

Fig. 12 Semisubmersible and symmetrical fluid domain modeled in ComFLOW

Fluid initial condition was set to a completely developed velocity field with the linear wave crest located at the domain center. As a consequence, one should notice that the first wave elevation peak is not a reliable value and the results should be considered only after the second wave crest passes the SS model position.

At the inlet boundary, linear wave inflow conditions were imposed. For computational reasons the domain size had to be truncated at a certain distance of the platform model. Therefore, a wall had to be positioned on the left side (positive y coordinate) and a full reflection condition was imposed as no wave absorbing boundary conditions are already implemented in the software for the side walls. On the right side boundary a symmetrical condition was implemented. At the outlet boundary, a Sommerfeld boundary condition was set to avoid wave reflections into the domain. This condition is set to absorb only the incident wave field and; therefore, neglects the waves diffracted by the body. All of these domain characteristics may not be enough to guarantee the complete absence of waves reflected by the side walls and their influence at the points of interest, although this influence is expected to be small.

The semisubmersible platform modeled in ComFLOW is situated in the center of the domain and was elaborated by the superposition of 12 bricks analytically implemented in the software: four bricks for the pontoons, four for the columns, and the others for the blisters installed. The semisubmersible modeled in ComFLOW is shown in Fig. 12.

The free surface elevation was monitored by seven numerical wave probes located at the same positions where the experimental wave probes were situated.

4 Fixed Model Tests Results and Comparison

Tests covered the range of wave steepness from 0.020 to 0.055 and the wave elevation was being monitored by seven wave probes as shown in Fig. 4. In order to focus on different phenomena the WPs were separated in three different groups: WP2, WP3, and WP4 located close to the stern columns front wall to provide results on the run-up effects, WP5 and WP6 to evaluate effects on the column corner, WP1 and WP7 along the hull centerline in between the bow and stern columns, respectively.

Results for wave run-up effects are presented in Figs. 13, 14, and 15 for WP2, WP3, and WP4, respectively. The results of these WPs seem identical, since locations of the respective measuring points are very close. WP3 and WP4 are located at the same x coordinate, slightly displaced from the right and left stern

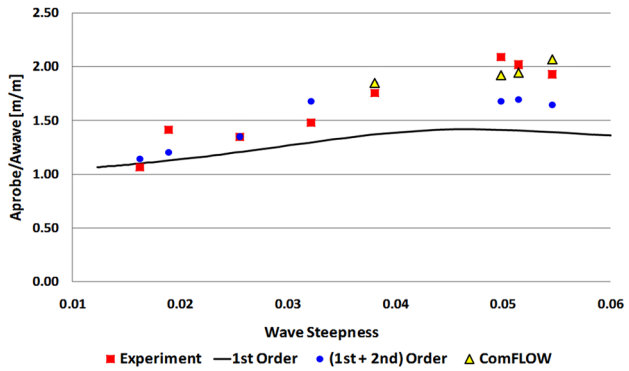

Fig. 13 Nondimensional wave elevation at WP2 (captive test)

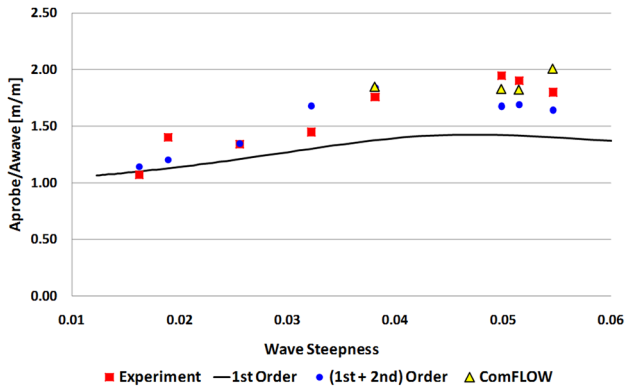

Fig. 14 Nondimensional wave elevation at WP3 (captive test)

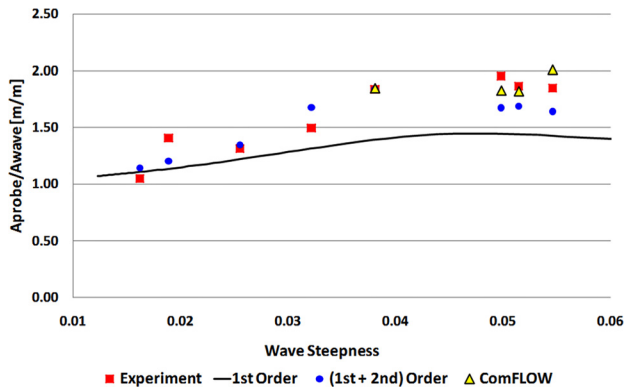

Fig. 15 Nondimensional wave elevation at WP4 (captive test)

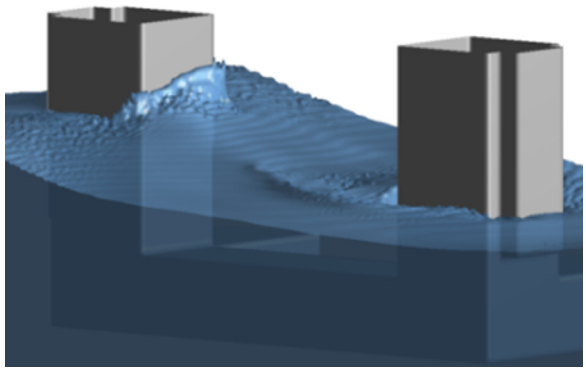

Fig. 16 Wave splash on the stern column in the ComFLOW model

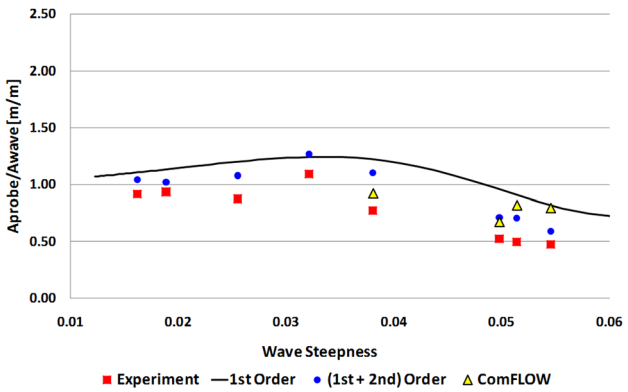

Fig. 17 Nondimensional wave elevation at WP5 (captive test)

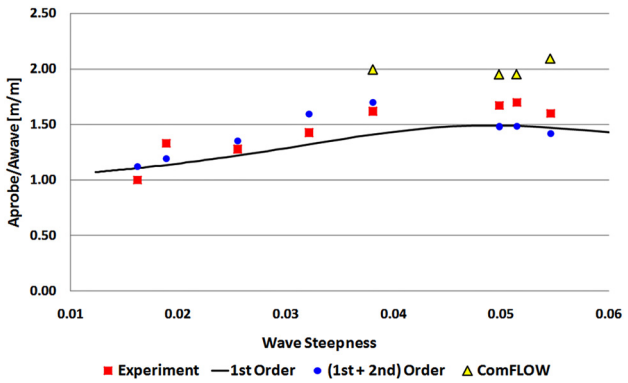

Fig. 18 Nondimensional wave elevation at WP6 (captive test)

columns, respectively, and WP2 is in the vicinity of the right stern column.

As expected, first order results agree well with the experimental values only for low wave steepness. On the other hand, for higher values of steepness, a large difference is observed and the second order and full nonlinear CFD solutions become more suitable. Improvements over the first order solution are clearly observed when second order effects are incorporated. Nonetheless, although the inclusion of the second order effects correctly recovers the amplitude trend with respect to the steepness, the ComFLOW results were clearly capable to represent the run-up effects more accurately. ComFLOW results also pointed out an interesting issue concerning the results for the largest wave steepness. It can be seen that nondimensional free surface elevations greater than 2.0 were predicted by the numerical model, although lower values were observed in the tests. The discrepancy may be related to the wave splash indicated by the simulations, which might also have rendered somewhat imprecise measurements from the wave probes. Figure 16 illustrates this phenomenon in a snapshot from the ComFLOW post processing tool.

Figures 17 and 18 present the results from the WP5 and WP6, respectively. Both WAMIT second order and ComFLOW lead to better agreement concerning the bow column corner (WP5), however ComFLOW results tend to overestimate the wave amplitude at the corner of the stern column, where the run-up effects are more pronounced.

The results of the WPs positioned between the columns in the centerline are illustrated in Figs. 19 and 20. ComFLOW predicted exactly the same values of free surface elevation at the WP1, whereas first and second order solutions presented some discrepancies.

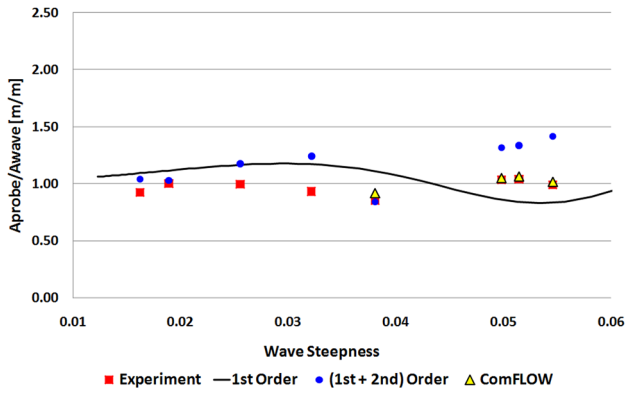

Fig. 19 Nondimensional wave elevation at WP1 (captive test)

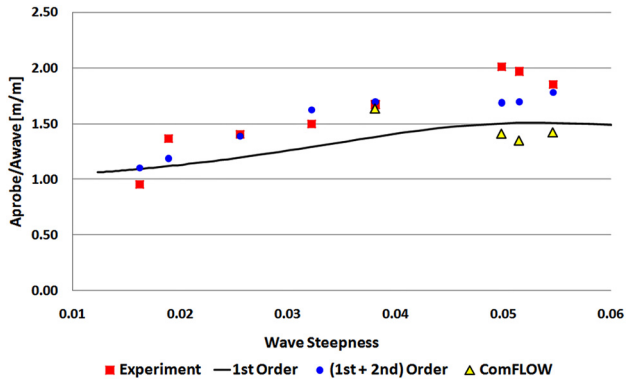

Fig. 20 Nondimensional wave elevation at WP7 (captive test)

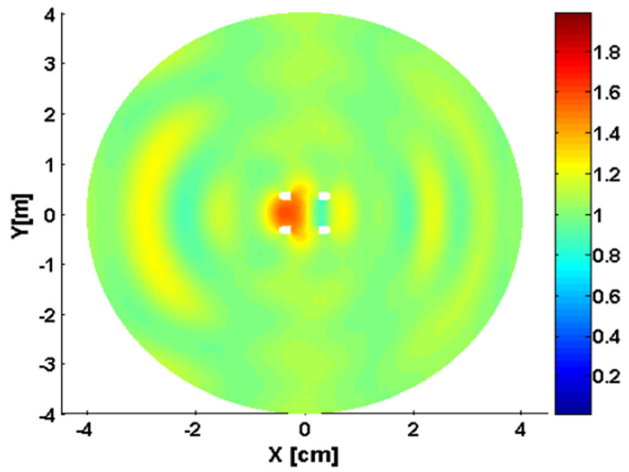

Fig. 21 Free surface elevation mapping around of the platform

Interesting aspects should be discussed concerning WP7. This WP is located in a region where the elevation is amplified, reaching values close to those observed in front of the columns. It may be realized that the numerical predictions agree reasonably well with the experiments for steepness below 4%. However, for higher values of steepness larger discrepancies are observed with both methods tending to underestimate the wave elevation, indicating a possible strong influence of nonlinear diffraction effects in this location. One explanation for the underestimated results predicted by ComFLOW may be the fact that the simulations were interrupted before a total developed diffracted field was established at this region; nevertheless future investigations still need to be performed in order to reach a conclusive explanation.

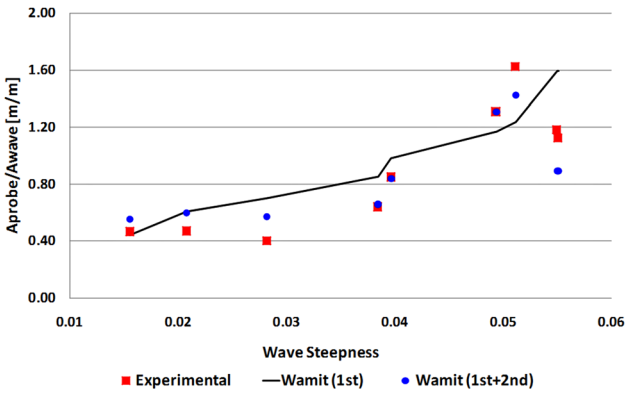

Fig. 22 Nondimensional wave elevation at WP2 (moored test)

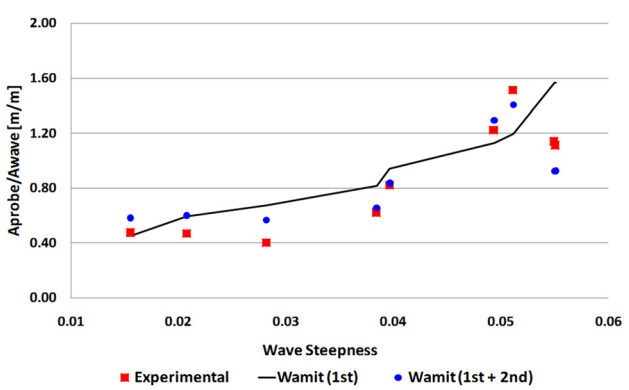

Fig. 23 Nondimensional wave elevation at WP3 (moored test)

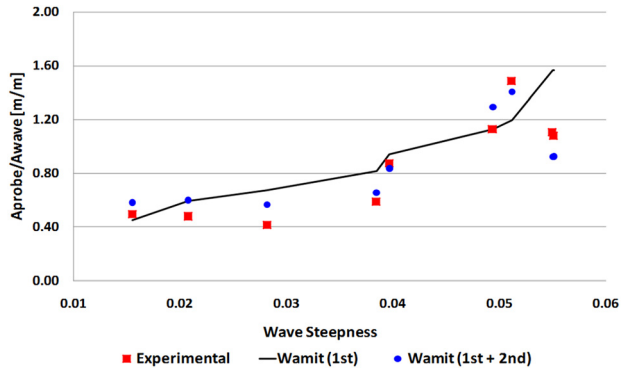

Fig. 24 Nondimensional wave elevation at WP4 (moored test)

Figure 21 illustrates the free surface elevation mapping, provided by WAMIT, around the platform for a steepness of 2.5% which is in the region of good agreement with the experiment. Through Fig. 21, it is possible to see that the amplification on the free surface really occurs between the stern columns, whereas an attenuation is observed at bow columns where was located the WP5 and WP1.

5 Moored-Model Tests Results and Comparison

Results presented in this section concern the tests conducted with the model moored in the simplified arrangement illustrated in Fig. 1. By direct comparison with those obtained with the fixed-model, it becomes clear that the model motions act favorably with respect to the air gap requirements, reducing the maximum wave elevation in all the monitored locations.

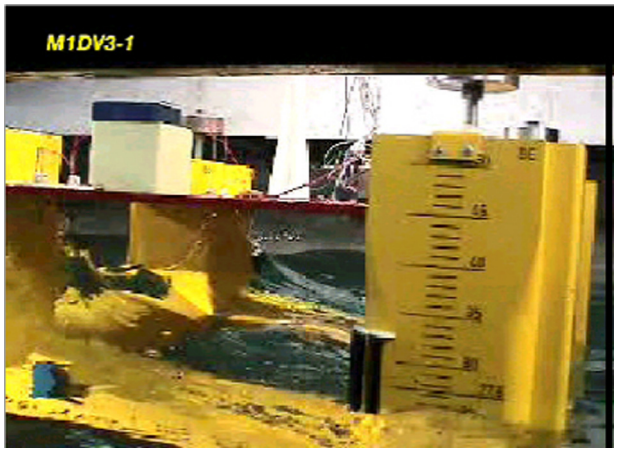

Fig. 25 Wave run-up (moored-model test)

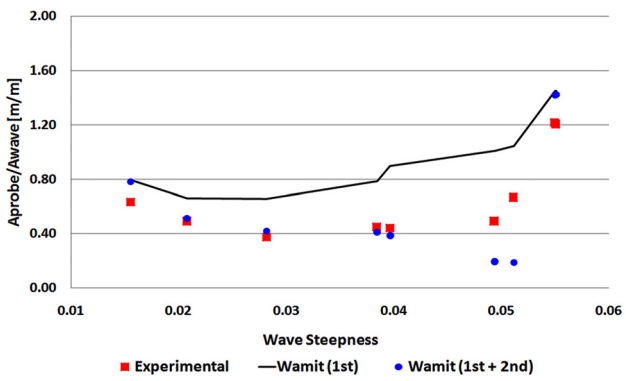

Fig. 26 Nondimensional wave elevation at WP5 (moored test)

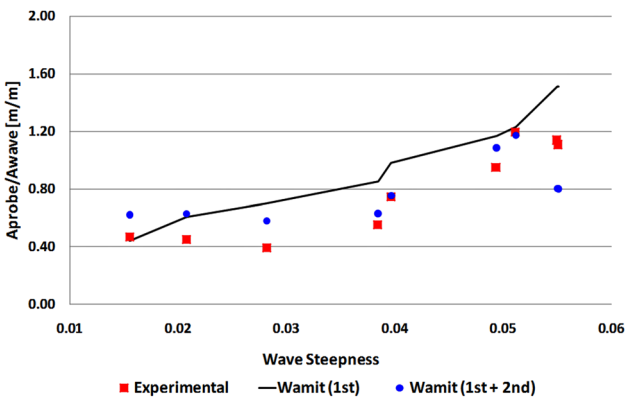

Fig. 27 Nondimensional wave elevation at WP6 (moored test)

As for the fixed model, tests with the moored model covered a range of wave steepness from 0.02 to 0.055. Both first and second order numerical analyses were performed using WAMIT®. The consideration of second order effects on the analysis is not restricted to the evaluation of the free surface elevation, as the difference frequency (mean) heave and pitch motions are also computed.

The results for WP2, WP3, and WP4 are presented in Figs. 22, 23, and 24, respectively. For these WPs, the wave run-up effects were clearly identified in the experiment, as shown in Fig. 25. As expected, extending the analysis to the second order significantly improves the results. Numerical predictions follow the experimental trends closely, even capturing the drop in amplitude observed for the steepest wave.

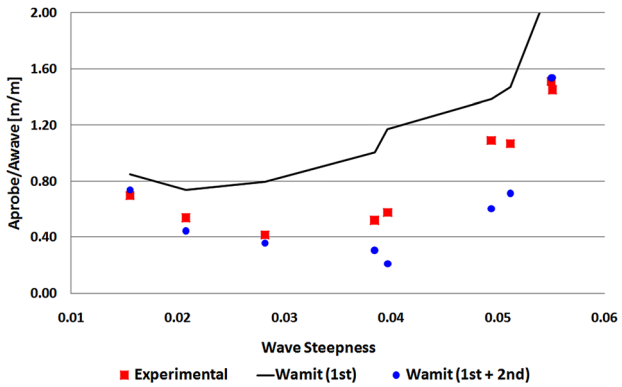

Fig. 28 Nondimensional wave elevation at WP1 (moored test)

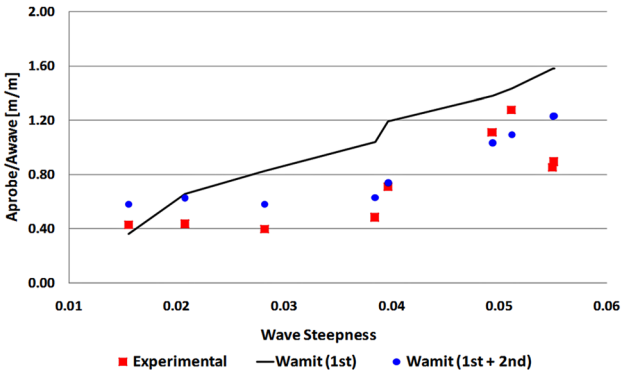

Fig. 29 Nondimensional wave elevation at WP7 (moored test)

Figures 26–29 bring the results for four other measurement points. In all cases, the influence of second order effects is indeed significant and renders better predictions of the wave elevation when compared to the experimental values. Regarding the WP7 position, it is also important to stress that the large amplifications observed with the model fixed practically disappear when the model is free to oscillate.

6 Conclusion

This paper addressed some fundamental studies on the wave run-up and air gap for a large semisubmersible unit. Tests with a small-scale model in two configurations (fixed and moored) under the action of regular waves were employed for the sake of comparison of numerical models. In these tests, free surface elevation was measured at seven different locations below the deck.

Results have shown that the WAMIT second order extension has clearly improved the results in comparison to the standard first order analysis for both fixed and moored situations. In addition, the VOF code ComFLOW simulations, compared to the fixed-model tests only, presented results even more precise, although the analysis demanded a long processing time. The moored-model simulations with ComFLOW still need to be investigated.

For the continuity of the ongoing research project, further studies will be performed concerning the wave run-up phenomenon and the statistics of extremes required for minimum air gap definition. As a first step, experimental results obtained in several different irregular wave tests will be analyzed and confronted to the numerical predictions to be executed via WAMIT first and second order modules. Advancing the CFD analysis, the ComFLOW model should be extended to evaluate the moored model situation for both, the regular wave tests already discussed in this paper and also extreme events observed along the irregular wave tests.

Acknowledgment

The authors gratefully acknowledge Petrobras for sponsoring this Research Project and also providing the experimental results. We also thank Dr. Bas Buchner of the MARIN for making ComFLOW code available to this study and Dr. Roel Luppes of the University of Groningen, The Netherlands, for the technical support. Finally, F.T.M. acknowledges FAPESP for his scholarship (Proc. No. 2007/05858-2).

References

[1] Stansberg, C. T., Baarholm, R., Kristiansen, T., Hansen, E. W. M., and Rortveit, G., 2005, "Extreme Wave Amplification and Impact Loads on Offshore Structures," Offshore Technology Conference, Houston, May 2–5.

[2] Danmeier, D. G., Seah, R. K. M., Finnigan, T., Roddier, D., Aubault, A., Vache, M., and Imamura, J. T., 2008, "Validation of Wave Run-Up Calculation Methods for a Gravity Based Structure," Proceedings of the ASME 27th International Conference on Offshore Mechanics and Arctic Engineering (OMAE2008), Estoril, Portugal, June 15–20.

[3] WAMIT, 2004, "WAMIT User Manual 6.2, 6.2PC, 6.2S, 6.2S-PC," WAMIT Inc., MA.

[4] Simos, A. N., Fujarra, A. L. C., Sparano, J. V., Umeda, C. H., and Rossi, R. R., 2006, "Experimental Evaluation of the Dynamic Air Gap of a Large-Volume Semi-Submersible Platform," Proceeding of the 25th International Conference on Offshore Mechanics and Artic Engineering (OMAE2006), Hamburg, Germany, June 4–9.

[5] Comflow V2.3, 2008, "Manual Comflow V2.3."

[6] Hirt, C. W., and Nichols, B. D., 1981, "Volume of Fluid (VOF) Method for the Dynamics of Free Boudaries," J. Comput. Phys., **39**, pp. 201–225.

[7] Pinkster, J. A., 1980, "Low Frequency Second Order Wave Exciting Forces on Floating Structures," Ph.D. thesis, Delft University of Technology, The Netherlands.

[8] Simos, A. N., Sparano, J. V., Aranha, J. A. P., and Matos, V. L. F., 2008, "2nd Order Hydrodynamic Effects on Resonant Heave, Pitch and Roll Motions of a Large-Volume Semi-Submersible Platform," Proceeding of the 27th International Conference on Offshore Mechanics and Artic Engineering (OMAE2008), Estoril, Portugal, June 15–20.

[9] Iwanowski, B., Lefranc, M., and Wemmenhove, R., 2009, "CFD Simulation of Wave Run-Up on a Semi-Submersible and Comparison With Experiment," Proceedings of the ASME 28th International Conference on Offshore and Artic Engineering (OMAE2009), Honolulu, HI, May 31–June 5.

[10] Kleefsman, K. M. T., Loots, G. E., Veldman, A. E. P., Buchner, B., Bunnik, T., and Falkenberg, E., 2005, "The Numerical Simulation of Green Water Loading Including Motions and Incoming Wave Field," Proceedings of the 24th International Conference on Offshore Mechanics and Artic Engineering (OMAE2005), Halkidiki, Greece, June 12–17.

[11] Bunnik, T., and Veldman, A., 2010, "Modelling the Effect of Sloshing on Ship Motions," Proceedings of the 29th International Conference on Offshore Mechanics and Artic Engineering (OMAE2010), Shanghai, China, June 6–11.

[12] Buchner, B., Bunnik, T. H. J., Fekken, G., and Veldman, A. E. P., 2001, "A Numerical Study on Wave Run Up on an FPSO Bow," Proceedings of the 20th International Conference on Offshore Mechanics and Artic Engineering (OMAE2001), Rio de Janeiro, Brazil, June 3–8.

[13] Loots, E., and Buchner, B., 2004, "Wave Run Up as Important Hydrodynamic Issue for Gravity Based Structures," Proceedings of the 23th International Conference on Offshore Mechanics and Artic Engineering (OMAE2004), Vancouver, Canada, June 20–25.

[14] Wellens, P. R., Pinkster, J. A., Veldman, A. E. P., and Huijsmans, R. H. M., 2007, "Numerical Wave Run Up Calculation on GBS Columns," Proceedings of the 17th International Offshore and Polar Engineering Conference (ISOPE2007), Lisbon, Portugal, July 1–6.